Received: 14 September 2016 | Accepted: 2 December 2016

DOI: 10.1111/jace.14710

ORIGINAL ARTICLE

Journal of the American Ceramic Society

Phase stability in scandia-zirconia nanocrystals

Robson L. Grosso[1,2] | Eliana N. S. Muccillo[1] | Ricardo H. R. Castro[2]

[1]Energy and Nuclear Research Institute, Sao Paulo, Brazil

[2]Department of Materials Science and Engineering & NEAT ORU, University of California-Davis, Davis, California

Correspondence
Ricardo H. R. Castro, Department of Materials Science and Engineering & NEAT ORU, University of California-Davis, One Shields Avenue, Davis, California
Email: rhrcastro@ucdavis.edu

Funding information
Fundação de Amparo à Pesquisa do Estado de São Paulo, Grant/Award Number: 2014/24022-6; National Science Foundation DMR Ceramics, Grant/Award Number: 1055504, 1609781.

Abstract

Scandia-zirconia system has great technological interest as it has the highest ionic conductivity among doped zirconia ceramics. However, polymorphism is the most important limiting factor for application of this material. Considering that there is a strong grain size dependence on phase transitions in this class of materials, mapping out the stable polymorph as a function of grain size and composition may lead to more efficient compositional design. In this article, the phase stability of zirconia-scandia nanocrystals was investigated based on experimental thermodynamic data. Exploiting recent advances in microcalorimetry, reliable surface energy data for five polymorphs of scandia-zirconia system: monoclinic, tetragonal, cubic, rhombohedral β and γ are reported for the first time. Combining surface energy values with bulk enthalpy data obtained from oxide melt drop solution calorimetry allowed us to create a predictive phase stability diagram that shows the stable zirconia polymorph as a function of composition and grain size of the specimen within the range of 0-20 mol% scandia.

KEYWORDS
nanomaterials, phase diagrams, scandium/scandium compounds, zirconia

1 | INTRODUCTION

Zirconia-based oxides have been extensively investigated for solid electrolyte applications in solid oxide fuel cells (SOFC). Among the zirconia-based materials, the highest ionic conductivity, one of the key properties for electrolytes, is encountered in scandia-stabilized zirconia (ScZ).[1,2] This system displays high oxygen conductivity, higher than yttria-stabilized zirconia itself, low electronic conductivity, and high stability when compared to other oxygen ion conductors. All these properties of ScZ are substantially originated from the similarity in the ionic radii of Sc^{3+} and Zr^{4+} ions,[1] making it a strong candidate for next generation SOFC operating at intermediate temperatures (600-800°C).[1,2]

However, polymorphism of scandia-zirconia combined with high cost of scandium limit its application. Its crystalline structure is considerably more complex than yttria-zirconia, and at least seven phases have been identified in the bulk phase diagram: monoclinic, tetragonal (t and t'), cubic, and three rhombohedral forms of different stoichiometry, $Sc_2Zr_7O_{17}$ (β), $Sc_2Zr_5O_{13}$ (γ), and $Sc_4Zr_3O_{12}$ (δ).[3,4] Moreover, a metastable tetragonal phase (t'') also has been reported.[5] Most works performed on scandia-zirconia have focused on stabilization of the highest ionic conductivity polymorph (fluorite-type cubic) at room temperature. It is likely that once polymorphism control is better understood, the high costs of scandium shall decrease following demand for its superior properties.

Cubic phase stabilization of scandia-zirconia has been achieved by introducing a second additive[6,7] or by decreasing grain size to the nanoscale.[5,8,9] The size effect on polymorphism of oxides has been extensively studied in the literature and relates to the role of surface energies in the total energy of the system. Because of its symmetry, cubic polymorphs tend to have lower surface energies, allowing an increased thermodynamic stability when the particle sizes are small. By using directly measured surface and bulk energies using microcalorimetry, Drazin and Castro[10,11] have recently created phase stability diagrams for both yttria-zirconia[10] and calcia-zirconia[11] systems that can accurately account for the observed polymorphic stability

crossovers observed at the nanoscale. The phase stability of scandia-zirconia nanopowders as a function of temperature has been partially investigated by Abdala et al.,[5,8] showing that size is indeed a strong component in defining stable polymorphs. Okamoto et al.[9] have also demonstrated the effect of sizes to obtain the cubic polymorph in scandia-zirconia by utilizing Spark Plasma Sintering, a densification method capable of minimizing coarsening during sintering. However, suitable systematic thermodynamic description of the problem was not provided, mostly due to the lack of accurate thermodynamic data.

The aim of this work is to directly measure the surface energies of the different polymorphs existing in the scandia-zirconia system, within the range of 0-20 mol% scandia, by applying water adsorption microcalorimetry theory and, in combination with high-temperature oxide melt drop solution calorimetry providing information on bulk enthalpy (along with entropic calculations), create a diagram of phase stability that enables prediction of the stable polymorph as a function of composition and grain size at room temperature. Note that although the energetic argument shall justify the stability of particular phases at given grain sizes, the phase stability of zirconia systems has also been discussed from a view point of the kinetic nucleation.[12,13] From a practical point of view, both energetic and kinetic approaches must be addressed to fully comprehend and control the polymorphism of zirconia and other oxides at the nanoscale.

2 | EXPERIMENTAL PROCEDURE

2.1 | Material synthesis

Scandium nitrate hydrate (99.9%, Alfa Aesar, Ward Hill, MA) and zirconyl nitrate hydrate (99% Sigma-Aldrich, St. Louis, MO) were used as starting materials for the synthesis of $(Sc_2O_3)_x(ZrO_2)_{1-x}$ ($0 \leq x < 20$) compounds. Nanostructured samples of scandia-zirconia were synthesized by reverse-strike coprecipitation method.[10,14] Stoichiometric amounts of the starting materials were dissolved in deionized water to form a clear, dilute solution. The concentration of the cation solution was verified by gravimetry and adjusted to 0.5 mol/L. This solution was dropped pointwise into a magnetically stirred 5 mol/L excess ammonium hydroxide solution. The resultant mixture was washed and centrifuged three times using water, ethanol (50%), and denatured ethanol to remove any residual ammonium on the precipitated hydroxide. The powder was subsequently dried at 100°C for 48 hour and grounded in an agate mortar. The dried hydroxide powders were calcined in a box furnace in several conditions to cause crystallization into the oxide and allow coarsening to different grain sizes.

2.2 | Electron probe microanalysis

Scandium and zirconium contents in the synthesized samples were measured by wavelength-dispersive X-ray spectroscopy electron probe microanalysis using a Cameca SX100 (Gennevilliers, France) microprobe at accelerating voltage of 15 kV, 10 nA beam current, and 5 μm beam size. Samples of each prepared composition were pressed into pellets, polished, and carbon-coated prior to electron microprobe analysis. Sample composition was calculated from an average of 10 data points.

2.3 | X-ray diffraction

X-ray diffraction (XRD) was used to determine crystallographic phase and grain size of calcined scandia-zirconia powders using a Bruker-AXS (Billerica, MA) D8 Advance diffractometer operated at an 40 kV accelerating voltage with 40 mA emission current with CuK_α radiation (λ=1.5405 Å). Data were acquired over a range of 2θ between 20° and 90° with a step size of 0.01° and a collection time of 0.4 s/step. The lattice parameters and grain size were calculated using JADE 6.1 software to perform a whole profile fitting refinement using a PDF#64-9607 for cubic, PDF#51-1603 for tetragonal, PDF#51-1602 for monoclinic, PDF#64-9610 rhombohedral β, and PDF#61-7752 rhombohedral γ. Silicon standard was mixed to ScZ powders in order to ensure accuracy in lattice parameter determination. PDF#27-1402 was used for silicon standard refinement.

2.4 | Nitrogen adsorption

The surface area (SA) of the scandia-zirconia nanopowders was measured using a Gemini VII sorption instrument (Micromeritics, Norcross, GA) according to Brunauer-Emmett-Teller (BET) method.[15] Five-point adsorption isotherms of the nitrogen were collected in the p/p_0 relative pressure range (where p_0 denotes the saturation pressure) of 0.05-0.3 at −196°C. Samples were degassed in a vacuum degassing station (VacPrep 061; Micromeritics) at 400°C for 12 hour prior all experiments. Uncertainties in surface area were less than 1% of the experimental values.

2.5 | Water adsorption microcalorimetry

The surface energy of nanoparticles was determined using a combination of two instruments: a water sorption system (WA) (ASAP2020; Micromeritics), equipped with turbo pumps for vacuum-cleaning the samples from residual water and capable of dosing micromoles of water step-

wise, attached to a Setaram SetSYS Evolution (Caluire, France) calibrated against the enthalpy of fusion of gallium metal. The sorption system is designed for fork-shaped glass tubes with two arms, where the sample is placed in only one of them and the other is kept empty to serve as reference. The calorimeter records the heat difference between the empty and sample-containing tubes during each water dose. Therefore, by combining the heat signals from the calorimeter and the dosing data (in terms of pressure and adsorbed quantity), the heat of adsorption of water molecules on the surface of powder can be measured as a function of relative pressure at 25°C. The instrument and methodology are described in detail elsewhere.[16,17.]

Two square meters of powder lightly pressed into a pellet was placed in the sample side of the tube. Samples were degassed at 400°C for 12 hour under vacuum to ensure an initial anhydrous surface condition (as confirmed by thermogravimetric, TG, experiments heating up the sample up to 1000°C and comparing the mass loss with the 400°C/12 hour condition) and small doses of water (2 μmol) were sequentially pumped into the system, automatically controlled by the ASAP instrumentation, while the corresponding heat flow was recorded by the calorimeter. The amount of water adsorbed on the empty fork tube was independently measured and used for correction of the total adsorbed amount.

The surface energy (SE) for each sample was determined using a custom written MATLAB 2010a function recently reported based on the Gibbs adsorption analysis—relating the SE with the heat of adsorption and respective adsorbed quantities.[18] To that end, the water adsorption curves were fitted using a modified Langmuir-BET adsorption curve:

$$\theta = \theta_c \frac{b\sqrt{k}}{1+b\sqrt{k}} + \theta_p \frac{ck}{(1-k)[1+(c-1)k]} \quad (1)$$

where θ_c and θ_p are the chemisorption and physisorption monolayer coverage, respectively, and b and c are unit-less fit parameters, and k is the relative pressure (p/p_0). The differential heats of adsorption data were fitted using an empirical relationship:

$$\frac{dH_R}{d\theta} = De^{-\frac{\theta}{d}} + \left.\frac{dH_{con}}{d\theta}\right|_{T_o,p_0} \quad (2)$$

H_R is the heat of adsorption and H_{con} is the enthalpy of liquefaction of water (condensation). The equation requires two parameters where d is a decay parameter and D is a fitting parameter with units in kJ/mol. After fitting, the surface energy was numerically computed using Equation 3, which has been previously demonstrated as quantitative correlation between the surface energy and water adsorption coverage:

$$SA\frac{d^2SE}{dx^2} = \frac{d\theta}{dk}\left\{\frac{d^2H_R}{d\theta^2}\frac{d\theta}{dk} + \frac{d\mu_{gas}}{dk} - SE\frac{d^2SA}{d\theta^2}\frac{d\theta}{dk} + \frac{dSE}{dk}\left[\frac{SA}{\theta} - 2\frac{dSA}{d\theta} + SA\frac{d^2\theta}{dk^2}\left(\frac{dk}{d\theta}\right)^2\right]\right\} \quad (3)$$

where SA is the surface area, SE is the surface energy, and μ_{gas} is the vapor chemical potential.

The equation was integrated from the boundary condition at saturation, where the surface energy of the system equals to the energy of liquefaction of water (SE=0.072 J/m^2), to vacuum using an integration step size of 5×10^{-10} starting with a relative pressure of 1-5.8 $\times 10^{-17}$ since this is the closest value to 1 that is still smaller than it is in a 32-bit programming. Surface energies under different water coverage can be obtained using this methodology by stopping the integration at the desired pressure.

2.6 | Oxide melt solution calorimetry

High-temperature oxide melt drop solution calorimetry was performed in a custom-built Tian-Calvet twin microcalorimeter described by Navrotsky.[19] Approximately 5 mg of nanopowders were lightly pressed into pellets, weighted, and dropped from room temperature into $3Na_2O{\cdot}4MoO_3$ melted solvent at 700°C. Oxygen flushing (40 mL/min) and bubbling (3.5 mL/min) through the system was used to ensure that the final oxygen state was constant and to further sample dissolution. Calorimeter calibration was performed using the heat content of α-Al_2O_3 pellets of similar weight. All samples were equilibrated in a 50% relative humidity environment for 72 hours prior to the experiments to establish a constant water content, which was determined by thermogravimetric experiments. At least eight drops of sample were performed in order to get statistically meaningful data. The heats of dissolution were treated with thermochemical cycles, in particular, to address the water desorption/evaporation energies. Drop solution (DS) experiments with bulk samples (calcined at 1500°C) were also performed to populate the thermochemical cycles.

3 | RESULTS AND DISCUSSION

3.1 | Structural characterization

Nanopowders of scandia-zirconia were successfully synthesized by reverse-strike coprecipitation method. A total of 13 compositions were prepared. Each composition is referred to as xScZ, where x is Sc_2O_3 content in mol%. Precursors of each composition were calcined in several conditions varying temperature and dwell time in order to obtain crystalline single-phase nanoparticles of each polymorph. Amorphous material was not investigated in this

work. Five polymorphs were found for the ScZ system within the range of 0-19.3 mol%, in agreement with the phase diagram for bulk-ScZ,[4] but as a function of both grain size and composition. Figure 1 shows representative XRD pattern of each crystalline structure (monoclinic, tetragonal, cubic, β, and γ) with respective PDF number. The reader is referred to the Supporting Information file for XRD patterns for all samples, plotted for the different grain sizes.

Monoclinic phase was detected in samples with scandia content smaller than 3.1 mol%. In these cases, tetragonal phase was stabilized for grain sizes smaller than 8 nm. Noteworthy, one of the main difficulties in interpreting the structural patterns is differing phases that have similar diffraction patterns due to broadening related to the small grain sizes. While monoclinic polymorph is generally easy to be identified, the difference between the tetragonal and cubic patterns becomes subtle when grain sizes are below ~10 nm. For instance, Figure 2 shows XRD patterns for zirconia containing 3.1ScZ with the respective crystallite size indicated for each pattern. It is evident that only the tetragonal polymorph exists for the samples with grain sizes 24.8 and 63.9 nm, where the tetragonal pattern can be identified by the double peaks around 60°. However, below ~10 nm, peak broadening prevents differentiation between cubic and tetragonal polymorphs based on this reference. Alternatively, a small peak around 43° is characteristic of the tetragonal phase, but this is also hardly observed due to broadening.

To resolve in between tetragonal and cubic phases, the lattice parameters determined for all samples with grain sizes below 10 nm (using PDF#51-1603 of tetragonal polymorph) are reported in Table 1 (actual sizes in Table 2). Fitting using tetragonal PDF file was performed in order to evaluate tetragonality (c/a' ratio) of nanopowders[10,20] and, thereby, evidence the difference between cubic and tetragonal polymorphs. A continuous decrease in c/a' ratio for increasing scandia content is observed, suggesting that samples in between 1.1 and 6.3 mol% are tetragonal when

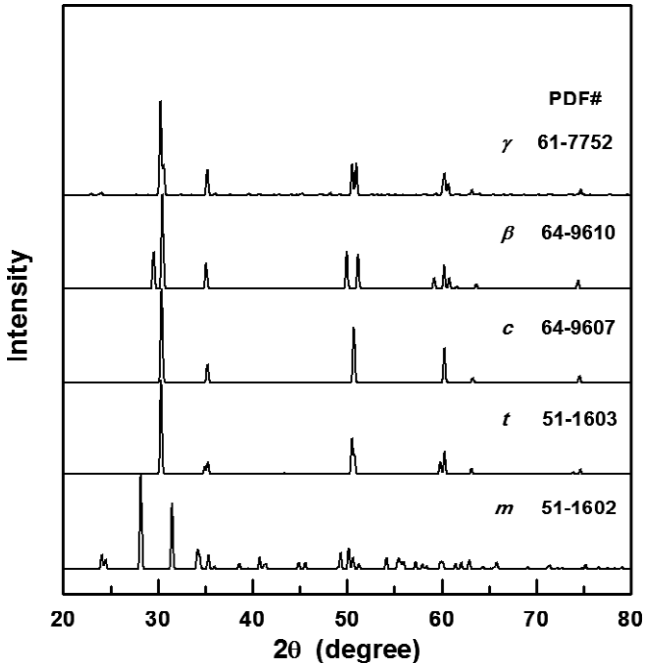

FIGURE 1 X-ray diffraction patterns of five polymorphs found for ScZ nanopowders, as indicated: monoclinic (*m*), tetragonal (*t*), cubic (*c*), rhombohedral (β and γ)

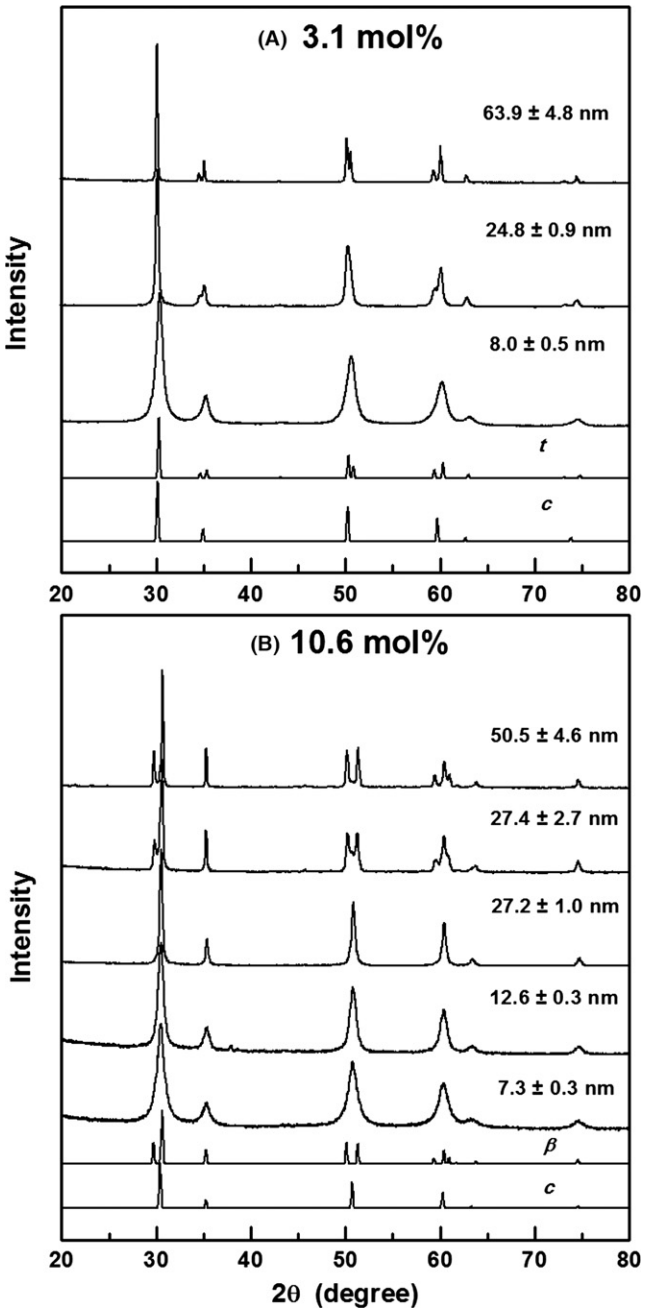

FIGURE 2 X-ray diffraction patterns of (A) 3.1ScZ and (B) 10.6ScZ nanopowders calcined at different conditions to allow variation in grain sizes

TABLE 1 Refined lattice parameters of nanopowders, with grain size below 10 nm, using tetragonal phase PDF#51-1603

Sc_2O_3 (mol%)	a (Å)	c (Å)	$a'=a\sqrt{2}$ (Å)	c/a'
1.1	3.5979	5.1502	5.0882	1.012
2.1	3.5958	5.1475	5.0852	1.012
3.1	3.5961	5.1376	5.0857	1.010
4.2	3.5949	5.1325	5.0840	1.010
6.3	3.5968	5.1252	5.0866	1.008
8.4	3.6019	5.0862	5.0939	0.998
10.6	3.5997	5.0829	5.0907	0.998
11.6	3.5974	5.0845	5.0875	0.999
12.9	3.5959	5.0582	5.0854	0.995
13.6	3.5914	5.0747	5.0790	0.999
14.3	3.5874	5.0870	5.0733	1.003
19.3	3.5824	5.0657	5.0663	1.000

grain sizes are below 10 nm, and cubic otherwise, since the ratio is close to unity.

The size-related phase stability occurring for either cubic or tetragonal against monoclinic is also observed for cubic against the rhombohedral phase in samples with higher scandia content. For instance, 10.6ScZ XRD patterns for different grain sizes are shown in Figure 2B. Apparently, the cubic phase is stabilized for grain sizes below 27 nm, which is very consistent with the literature reporting on c-β phase transition for 10ScZ nanofibers (26 nm).[21] Similar behavior was observed for zirconia containing 11.6 and 12.9 mol% scandia. For samples with higher scandia content, the rhombohedral γ polymorph was detected instead of the β phase, but having a similar tendency for stability of the cubic polymorph as grain sizes decrease.

The summary of experimental data for each sample studied in this work is listed in Table 2. The results are separated according to crystalline structure. Although it would be possible to draw a diagram of polymorphic stability as a function of grain size simply based on the presented data, the uncertainty in the intermediate compositions and sizes disable a reliable diagram with predictive capabilities. Moreover, it is not possible to assure that the samples are indeed in a metastable condition, and hence a thermodynamic analysis is required.

3.2 | Thermodynamic analysis

The phase stability of nanomaterials can be evaluated from a thermodynamic perspective by introducing a surface excess term to the Gibbs free energy equation to account for the large surface areas:

$$G = H - T.S + \mathrm{SA.SE} \quad (4)$$

where H is the molar enthalpy in kJ/mol, T is the absolute temperature in K, S is the molar entropy in J/mol, SA is the surface area in m^2/mol, and SE is the surface energy in J/m^2. At chemical equilibrium between any two polymorphs ($p1$ and $p2$), the Gibbs free energy should be zero. By assuming that there is no change in surface area of the system during the $p1$-$p2$ phase transformation, Equation 5 can be written as:

$$\Delta G_{p1\to p2} = \Delta H_{p1\to p2} - T.\Delta S_{p1\to p2} + \mathrm{SA.SE}_{p1\to p2} = 0 \quad (5)$$

and rearranged, as a function of SA, it becomes:

$$\mathrm{SA} = \frac{\left(H_{p2} - H_{p1}\right) - T\left(S_{p2} - S_{p1}\right)}{\left(\mathrm{SE}_{p1} - \mathrm{SE}_{p2}\right)} \quad (6)$$

The equation suggests there is a critical surface area (and consequently, grain size if particles are isotropic) for the transition that is not only dependent on the bulk enthalpies or entropies, but on the surface energy difference between the phases. In order to find a relation between the grain size and thermodynamic properties, considering ideal spherical particles, the surface area term (in m^2/mol) as a function of grain size (d) can be expressed by:

$$\mathrm{SA} = \frac{6M}{d.\rho} \quad (7)$$

where M is the molar mass in g/mol and ρ is the density in g/cm^3. Finally, Equations 6 and 7 can be combined and rearranged as follows:

$$d = \frac{6.M\left(\mathrm{SE}_{p1} - \mathrm{SE}_{p2}\right)}{\rho\left[\left(H_{p2} - H_{p1}\right) - T\left(S_{p2} - S_{p1}\right)\right]} \quad (8)$$

Thus, to assess the critical particle (grain) size (d) of the phase transition, reliable data on the surface energy, bulk enthalpy, and entropy of all the polymorphs are required. As mentioned in the Introduction section, the oxide surface energies have been historically the most challenging parameter to measure. However, with recent advances in microcalorimetry, it is possible to obtain accurate surface energy data which allow building of predictive diagrams for nanocrystals.

3.3 | Water adsorption microcalorimetry

In order to determine the surface energy of the different polymorphs of ScZ, water adsorption was performed on the anhydrous nanoparticles (dried using degassing procedure described in the Experimental Procedure section). Figure 3 shows the experimental data for the quantity of water adsorption and respective enthalpy for all studied ScZ

TABLE 2 Summary of experimental data for each studied sample

Sc_2O_3 (mol%)	Calcination (°C/h)	Grain Size (nm)	*SA* (m^2/g)	H_2O (wt%)	ΔH_{ads} (kJ/mol)	*SE* (J/m^2)	ΔH_{bulk} (kJ/mol)
Monoclinic							
0	1100/12	31.5 ± 1.8	2.7	0	−60.5 ± 1.5	0.78 ± 0.07	19.5 ± 0.3
1.1	1100/12	30.4 ± 1.4	3.6	0.2	−60.7 ± 1.3	0.88 ± 0.05	16.9 ± 1.3
2.1	1500/15	—	—	0	—	—	6.7 ± 0.7
Tetragonal							
1.1	450/0	7.1 ± 0.3	139.1	7.4	−64.7 ± 0.8	0.85 ± 0.02	−6.6 ± 1.3
2.1	500/2	7.8 ± 0.5	117.6	6.5	−67.8 ± 1.2	0.87 ± 0.05	−11.6 ± 1.5
3.1	500/2	8.0 ± 0.5	114.5	7.1	−73.0 ± 1.6	0.85 ± 0.04	−14.9 ± 2.0
4.2	500/2	7.9 ± 0.2	124.7	6.1	−73.7 ± 1.6	0.88 ± 0.04	−7.5 ± 2.1
6.3	500/2	7.9 ± 0.4	119.7	6.2	−71.0 ± 1.5	0.83 ± 0.04	−3.3 ± 1.2
Cubic							
8.4	500/2	7.7 ± 0.6	120.3	10.6	−66.7 ± 1.2	0.81 ± 0.04	−8.3 ± 0.3
10.6	500/2	7.3 ± 0.5	120.6	7.0	−70.5 ± 1.5	0.75 ± 0.04	−16.1 ± 1.8
11.6	500/2	6.7 ± 0.4	139.7	7.2	−69.3 ± 1.6	0.76 ± 0.04	−14.1 ± 2.2
12.9	500/2	5.2 ± 0.8	145.6	8.8	−64.0 ± 1.0	0.74 ± 0.03	−23.5 ± 1.2
13.6	500/2	5.1 ± 0.7	150.2	7.8	−65.6 ± 1.3	0.73 ± 0.03	−21.1 ± 1.5
14.3	500/2	4.9 ± 0.8	147.1	7.4	−67.2 ± 1.1	0.78 ± 0.03	—
19.3	500/2	4.7 ± 0.3	143.9	8.3	−69.9 ± 1.5	—	−31.8 ± 2.0
Rhombohedral β							
10.6	1150/12	50.5 ± 4.6	1.2	0	—	3.35 ± 0.30[a]	−2.3 ± 1.2
11.6	1000/10	30.8 ± 3.2	2.3	0	—	4.35 ± 0.35[a]	2.0 ± 2.5
12.9	1300/24	62.2 ± 5.6	0.3	0	—	4.40 ± 0.32[a]	−3.9 ± 0.2
Rhombohedral γ							
13.6	900/2	28.5 ± 2.0	16.3	0.8	—	2.36 ± 0.30[a]	−2.5 ± 1.0
14.3	900/2	35.6 ± 3.3	4.7	0	—	2.36 ± 0.30[a]	−4.3 ± 2.5
19.3	900/2	24.8 ± 2.3	19.0	0.8	—	2.51 ± 0.25[a]	−7.7 ± 1.0

[a]Calculated from linear trends of enthalpy of drop solution as a function of surface area.

samples. Note that only the samples with a single polymorph were used in this study. In Figure 3A, water coverage is plotted as a function of relative pressure. The shape of the curve consists of three stages, consistently with recent literature reports for other oxides.[10,11,16-18] Initially, there is a rapid increase in the adsorbed water at small relative pressures (<0.02) associated to the high reactivity of the anhydrous surface. This first stage is followed by an isotherm with smaller slope for pressures up to about 0.4, which increases again to a third stage until reaching the limit of the instrumentation at a relative pressure of 0.72. Note that there is a gap of points at about 0.23 of relative pressure, this is caused by an instrument pressure gage automatic change, and has insignificant consequences on data analysis.

The enthalpy of water adsorption as a function of water coverage is presented in Figure 3B. All curves show a typical behavior with highly exothermic adsorption at low coverages, and a systematic decrease followed by leveling.[18] The enthalpy becomes less exothermic with increase of water layers until saturation of the nanoparticles, where enthalpy reaches −44 kJ/mol (dotted line), which is the enthalpy of liquefaction of water. It is interesting to note that, although the curves for all investigated compositions and polymorphs obtained by water adsorption microcalorimetry experiments have a quite similar shapes, significant differences in absolute values and slopes were encountered. The differences are not clear due to curves overlapping.

The anhydrous surface energy of ScZ nanoparticles was determined by combining the heat of adsorption and isotherm experimental data to solve the differential equation presented in the experimental session using a custom written MATLAB 2010a function as described in detail previously.[18] Experimental data for each of the polymorphs were fitted with Equations 1 and 2 (adsorption curve and heat of adsorption curve, respectively), and plugged into the differential Equation 3 for solving. Good agreement

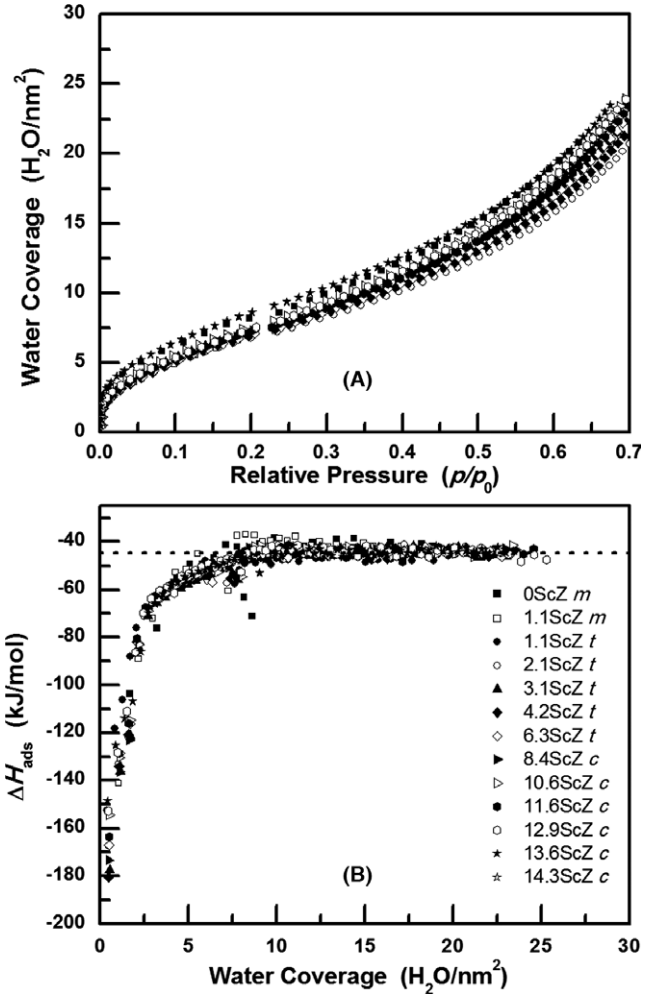

FIGURE 3 Water adsorption microcalorimetry data for monoclinic, tetragonal, and cubic phases of the ScZ system. A, Water coverage isotherm as a function of relative pressure. B, Enthalpy of water adsorption as a function of water coverage on the ScZ nanoparticles

between regression functions fit and experimental data has been demonstrated for several materials when using the proposed Equations 1 and 2, and similar results were obtained in the present work.[10,11,18] The calculated surface energy values of all studied polymorphs are finally presented in Table 2.

Although the water adsorption technique was efficient in delivering surface energy data for most samples, a different methodology needed to be adopted for both β and γ phases. This is because the water adsorption microcalorimetric experiments require specimens with relatively large surface areas, an inherent problem for the rhombohedral structures that were only stable when the surface areas were significantly small (Table 2).

Therefore, the surface energies for β and γ phases were calculated from oxide melt solution calorimetry linear trends as a function of surface area of the cubic polymorph and the definition of the critical specific surface area for transformation described in Equation 6. The difference between the enthalpy of drop solution (ΔH_{DS}) of bulk and nanosamples, corrected for water content, arises from the surface energy term alone[22]:

$$\Delta H_{DS,\,nano} = \Delta H_{bulk} - SE.SA \tag{9}$$

Thus, by using the surface energy obtained from water adsorption microcalorimetry and the enthalpy of drop solution for cubic polymorphs (Table 2), one may use actual experimentally observed specific surface areas for the *c*-β and *c*-γ phase transitions determined by step growth and phase analyses, and use the ΔH_{bulk} of the rhombohedral polymorphs to calculate the surface energies for each polymorph. This approach has been used for surface energy calculations of other materials.[22] The values used for SE calculations are presented in Table 3, and the surface energy data are included in Table 2.

Figure 4 shows anhydrous surface energy values of the five polymorphs plotted against Sc_2O_3 content. Regression fit for each polymorph was performed using Origin 8.0 software. Values for tetragonal and cubic phases are below 0.9 J/m^2, and show a systematic decrease with increasing scandia content. Higher values obtained for β and γ phases are consistent with the existence of these phases only at relatively large grain sizes, and show consistency with bulk-phase diagrams for scandia-zirconia.[4]

The surface energy regression fits in J/m^2 determined for each polymorph are presented below as a function of *x*, concentration of Sc_2O_3 in mol%.

$$SE_m = (0.732) + (0.177)x \tag{10}$$

$$SE_t = (0.877) + (-0.00718)x \tag{11}$$

$$SE_c = (1.153) + (-0.130)x + (0.00536)x^2 \tag{12}$$

TABLE 3 Grain size, specific surface area, and enthalpy of drop solution of *c*-β and *c*-γ phase transitions used for calculation of the surface energies of rhombohedral samples

Sc_2O_3 (mol%)	Grain Size (nm)	*SA* (m^2/mol)	$\Delta H_{DS,\,nano}$ (kJ/mol)
c-β phase transition			
10.6	27	~4400	−17
11.6	27	~4400	−20
12.9	27	~4400	−23
c-γ phase transition			
13.6	13	~9100	−28
14.3	10	~1200	−33
19.3	8	~1450	−44

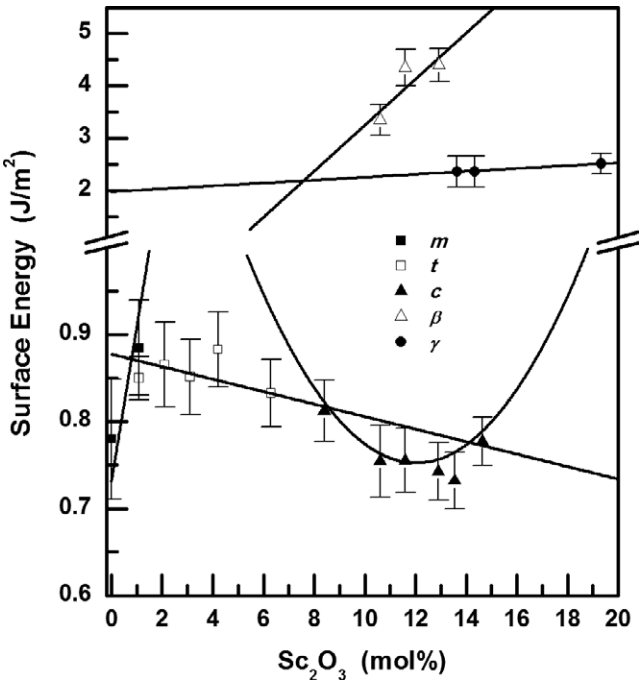

FIGURE 4 Surface energy values for five polymorphs as a function of Sc_2O_3 content for the different polymorphs, as indicated in the legend

$$SE_\beta = (-1.153) + (0.440)x \quad (13)$$

$$SE_\gamma = (1.973) + (0.0277)x \quad (14)$$

Using these equations, one may calculate the surface energy changes during a particular phase transition as a function of composition.

3.4 | High-temperature calorimetry

In order to build a comprehensive phase diagram, accurate enthalpy data for bulk stability of each polymorph are required, which was obtained using high-temperature oxide melt drop solution calorimetry. During a typical drop solution experiment, the resultant heat effect of nanoparticles with large surface area, referred to further as "the drop solution enthalpy," consists of the heat content of the sample from room temperature to the calorimeter temperature, the heat of sample dehydration, the surface energy, and the heat of dissolution. Thus, enthalpy corrections using an appropriate thermochemistry cycle are required to extract bulk enthalpy trends. For samples with large grain sizes (bulk materials), the heat of sample dehydration as well as surface energy contributions are negligible. The thermochemical cycle is given in Table 4.

Combining thermogravimetry, water adsorption, and surfaces area and energy data (listed in Table 2), the enthalpy of dissolution for each prepared sample was determined. Corrected heat of drop solution for each sample is presented in Table 2.

TABLE 4 Thermochemical cycle used for water correction of drop solution data

$ScZ_{(nano,\ 25°C)}{\cdot}xH_2O_{(ads,\ 25°C)} \rightarrow ScZ_{(soln,\ 700°C)} + xH_2O_{(g,\ 700°C)}$	$\Delta H_1 = \Delta H_{DS}$
$xH_2O_{(l,\ 25°C)} \rightarrow xH_2O_{(g,\ 700°C)}$	$\Delta H_2 = x(25.0 \pm 0.1)$ kJ/mol
$xH_2O_{(ads,\ 25°C)} \rightarrow xH_2O_{(l,\ 25°C)}$	$\Delta H_3 = -x\Delta H_{ads}$
$ScZ_{(nano,\ 25°C)} \rightarrow ScZ_{(bulk,\ 25°C)}$	$\Delta H_4 = -SE.SA$
$ScZ_{(bulk,\ 25°C)} \rightarrow ScZ_{(soln,\ 700°C)}$	$\Delta H_5 = \Delta H_{bulk}$
$\Delta H_1 = \Delta H_2 + \Delta H_3 + \Delta H_4 + \Delta H_5$	$\Delta H_5 = \Delta H_{bulk}$

x = total water content determined by thermogravimetry.

The enthalpy of drop solution of pure zirconia measured in this work was 19.5 ± 0.3 kJ/mol, which is in agreement with previously reported value for monoclinic ZrO_2.[23] Figure 5 shows the corrected enthalpy of drop solution (bulk) for the five polymorphs against Sc_2O_3 content. The measured enthalpies of tetragonal polymorph are less endothermic than monoclinic phase. This indicates higher stability of the monoclinic phase for low scandia content, which is also consistent with XRD results for compositions of 1.1 and 2.1 mol% scandia.

The studied rhombohedral structures presented similar energies but were regression fitted with quadratic equation instead of a linear function as for γ, for consistency with the observed microstructures and literature results. Enthalpy of drop solution for all these structures of ScZ system, except for γ polymorph, is being reported for the first time, but the results obtained for rhombohedral γ are in full agreement with other literature.[24]

The regression fits of enthalpy of drop solution obtained for each polymorph in kJ/mol are presented below as a function of x, Sc_2O_3 content in mol%.

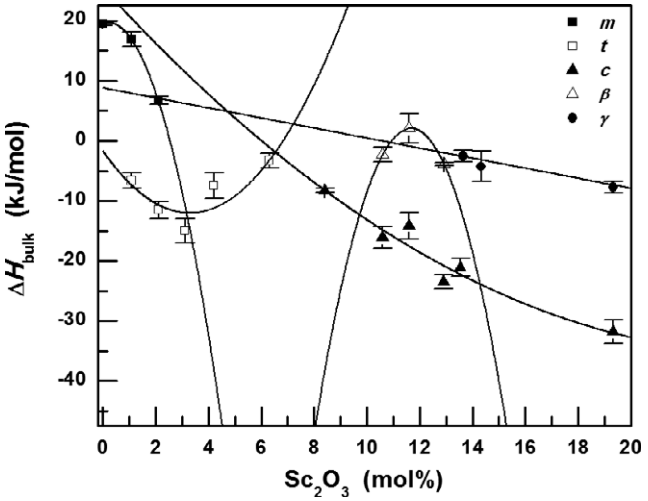

FIGURE 5 Corrected enthalpy of drop solution for five polymorphs as a function of Sc_2O_3 content as indicated in the legend

$$H_m = (19.48) + (1.495)x + (-3.603)x^2 \quad (15)$$

$$H_t = (-1.708) + (-6.279)x + (0.957)x^2 \quad (16)$$

$$H_c = (25.476) + (-4.814)x + (0.0951)x^2 \quad (17)$$

$$H_\beta = (-513.556) + (88.326)x + (-3.783)x^2 \quad (18)$$

$$H_\gamma = (8.784) + (-0.836)x \quad (19)$$

Similarly to surface energy data, fitting equations of enthalpy of drop solution may be used to determine heats of phase transformations for $m \rightarrow t$, $c \rightarrow t$, $c \rightarrow \beta$, and $c \rightarrow \gamma$.

3.5 | Entropy

The other important term in phase transition thermodynamics is the entropy. The entropy of each phase transition mentioned above can be determined using the enthalpy of phase transition from Jacobson et al. experiments for pure zirconia, which include $\Delta S_{m \rightarrow t}$=4.10 J/K·mol and $\Delta S_{t \rightarrow c}$=2.29 J/K·mol.[25] For cubic-rhombohedral phase transition, the values are $\Delta S_{c \rightarrow \beta}$=1.23 J/K·mol and $\Delta S_{c \rightarrow \gamma}$=1.36 J/K·mol according to Fujimori et al.[26] and Simoncic and Navrotsky,[24] respectively. Due to the fact that the entropy does not scale excessively with temperature, these values are assumed to be close to room-temperature values. Changes in entropy due to scandia additions were modeled by a regular solution model described in equation below[10]:

$$\Delta S_{\text{Regular}} = -R[x \ln(x) + (1-x)\ln(1-x)] \quad (20)$$

where x is the fractional scandia content in mol% and R is the gas constant.

Although replacement of zirconium by scandium ions promote sublattices distortions due to increase in oxygen vacancy concentration, this equation does not take defect associations into account. These defects could compromise randomness of mixing in this system, and consequently overestimate configurational entropy. However, the entropy contribution is very minimal and do not compromise the stability trends defined by the enthalpic terms. Hence, the approaches used in this work are consistent and appropriate for the determination of the nanophase diagram.

3.6 | Diagram of phase stability

Figure 6 shows the grain size diagram of phases for the scandia-zirconia system for the room temperature. The lines were calculated according to Equation 8. Each region corresponds to the stable polymorph given a grain size and scandia content. The ordinate axis is shown in a log base 10 scale to observe many orders of magnitude in grain size.

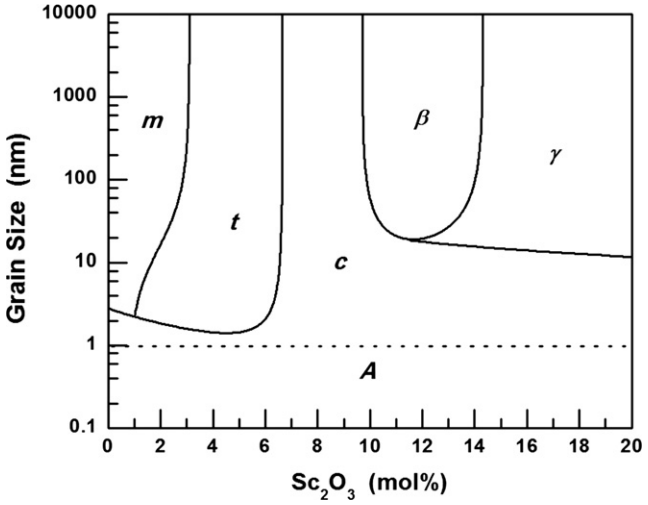

FIGURE 6 Diagram of phase stability as a function of grain size and scandia content. Areas of phase stability are indicated in the plot by the respective symbol. Amorphous area is for reference only

Although amorphous (A) materials were not studied in this work, dashed line represents a possible limit for amorphous-cubic phase transition. This limit was estimated based on lattice parameter of the cubic polymorph. However, grain sizes around 0.1 nm are impracticable for zirconia-based materials since the ionic radius of oxygen is 0.142 nm. Thus, the amorphous range in the graph can be considered a region where there are two possibilities, amorphous or without physical meaning. Since the nanophase diagram was designed for room-temperature applications (298 K), temperature dependencies are not considered.

Results encountered for pure zirconia suggested stabilization of the monoclinic polymorph above approximately 5 nm, in agreement to nanophase diagram published recently for yttria-zirconia.[10] Interestingly, the diagram is very consistent to the phase analysis of the as-synthesized samples. For example, 2.1ScZ shows a tetragonal-monoclinic phase transformation for grain sizes around 25 nm, while there is cubic phase stability in a wide grain size range around 8 mol%.[27] For zirconia containing 10.6, 11.6, and 12.9 mol% scandia, phase transition occurs around 27 nm (Table 3). The behavior found for c-γ, (a line with negative slope) is in agreement with results listed in Table 3. Good agreement with recently reported data for the scandia-zirconia nanomaterials is observed, where it has been shown that phase stability is strongly dependent on the grain size.[5,8,21,27]

4 | CONCLUSION

Unprecedented phase diagram at the nanoscale of grain size as a function of composition based on thermodynamic data

were successfully built for scandia-zirconia system. This result shows that thermodynamic data are a powerful predictive tool successfully applied to scandia-zirconia with high degree of accuracy. The diagram reveals that the surface energies are important contributions to the thermodynamic metastability of polymorphs and add to the conventional bulk phase diagrams in order to promote improvement in technological applications.

ACKNOWLEDGMENTS

The authors gratefully acknowledge FAPESP (2014/24022-6) and National Science Foundation DMR Ceramics (1055504, 1609781) for the support provided for this work.

REFERENCES

1. Badwal SPS, Ciacchi FT. Oxygen-ion conducting electrolyte materials for solid oxide fuel cells. *Ionics*. 2000;6:1–21.
2. Fergus JW. Electrolytes for solid oxide fuel cells. *J Power Sources*. 2006;162:30–40.
3. Fujimori H, Yashima M, Kakihana M, Yoshimura M. Structural changes of scandia-doped zirconia solid solutions: Rietveld analysis and Raman scattering. *J Am Ceram Soc*. 1998;81:2885–2893.
4. Ruh R, Garrett HJ, Domagala RF, Patel VA. The system zirconia-scandia. *J Am Ceram Soc*. 1977;60:399–403.
5. Abdala PM, Craievich AF, Fantini MCA, Temperini MLA, Lamas DG. Metastable phase diagram of nanocrystalline ZrO_2-Sc_2O_3 solid solutions. *J Phys Chem C*. 2009;113:18661–18666.
6. Arachi Y, Asaia T, Yamamoto O, et al. Electrical conductivity of ZrO_2-Sc_2O_3 doped with HfO_2, CeO_2, and Ga_2O_3. *J Electrochem Soc*. 2001;148:A520–A523.
7. Grosso RL, Muccillo R, Muccillo ENS. Stabilization of the cubic phase in zirconia-scandia by niobium oxide addition. *Mater Lett*. 2014;134:27–29.
8. Abdala PM, Fantini MCA, Craievich AF, Lamas DG. Crystallite size-dependent phases in nanocrystalline ZrO_2-Sc_2O_3. *Phys Chem Chem Phys*. 2010;12:2822–2829.
9. Okamoto M, Akimune Y, Furuya K, Hatano M, Yamanaka M, Uchiyama M. Phase transition and electrical conductivity of scandia-stabilized zirconia prepared by spark plasma sintering process. *Solid State Ionics*. 2005;176:675–680.
10. Drazin JW, Castro RHR. Phase stability in nanocrystals: a predictive diagram for yttria-zirconia. *J Am Ceram Soc*. 2015;98:1377–1384.
11. Drazin JW, Castro RHR. Phase stability in calcia-doped zirconia nanocrystals. *J Am Ceram Soc*. 2016;99:1778–1785.
12. Mitsuhashi T, Ichihara M, Tatsuke U. Characterization and stabilization of metastable tetragonal ZrO_2. *J Am Ceram Soc*. 1974;57:97–101.
13. Heuer AH, Claussen N, Kriven WM, Ruhle M. Stability of tetragonal ZrO_2 particles in ceramic matrices. *J Am Ceram Soc*. 1982;65:642–650.
14. Quach DV, Castro RHR. Direct measurement of grain boundary enthalpy of cubic yttria-stabilized zirconia by differential scanning calorimetry. *J Appl Phys*. 2012;112:3–8.
15. Brunauer S, Emmett PH, Teller E. Adsorption of gases in multimolecular layers. *J Am Chem Soc*. 1938;60:309–319.
16. Castro RHR, Quach DV. Analysis of anhydrous and hydrated surface energies of gamma-Al_2O_3 by water adsorption microcalorimetry. *J Phys Chem C*. 2012;116:24726–24733.
17. Ushakov SV, Navrotsky A. Direct measurements of water adsorption enthalpy on hafnia and zirconia surface using novel design for gas adsorption microcalorimetry. *Appl Phys Lett*. 2005;87:164103.
18. Drazin JW, Castro RHR. Water adsorption microcalorimetry model: deciphering surface energies and water chemical potentials of nanocrystalline oxides. *J Phys Chem C*. 2014;118:10131–10142.
19. Navrotsky A. Progress and new directions in high temperature calorimetry. *Phys Chem Miner*. 1977;2:89–104.
20. Krogstad JA, Lepple M, Gao Y, Lipkin DM, Levi CG. Effect of yttria content on the zirconia unit cell parameters. *J Am Ceram Soc*. 2011;94:4548–4555.
21. Yao L, Liu W, Ou G, Nishijima H, Pan W. Phase stability and high conductivity of ScSZ nanofibers: effect of the crystallite size. *J Mater Chem A*. 2015;3:10795–10800.
22. Sahu SK, Maram PS, Navrotsky A. Thermodynamics of nanoscale calcium and strontium titanate perovskites. *J Am Ceram Soc*. 2013;96:3670–3676.
23. Radha AV, Bomati-Miguel O, Ushakov SV, Navrotsky A, Tartaj P. Surface enthalpy, enthalpy of water adsorption, and phase stability in nanocrystalline monoclinic zirconia. *J Am Ceram Soc*. 2009;92:133–140.
24. Simoncic P, Navrotsky A. Systematics of phase transition and mixing energetics in rare earth, yttrium, and scandium stabilized zirconia and hafnia. *J Am Ceram Soc*. 2007;90:2143–2150.
25. Jacobson NS, Liu ZK, Kaufman L, Zhang F. Thermodynamic modeling of the $YO_{1.5}$-ZrO_2 system. *J Am Ceram Soc*. 2004;87:1559–1566.
26. Fujimori H, Yashima M, Kakihana M, Yoshimura M. β-cubic phase transition of scandia-doped zirconia solid solution: calorimetry, X-ray diffraction, and Raman scattering. *J Appl Phys*. 2002;91:6493–6498.
27. Xu G, Zhang YW, Liao CS, Yan CH. Doping and grain size effects in nanocrystalline ZrO_2-Sc_2O_3 system with complex phase transitions: XRD and Raman studies. *Phys Chem Chem Phys*. 2004;6:5410.

How to cite this article: Grosso RL, Muccillo ENS, Castro RHR. Phase stability in scandia-zirconia nanocrystals. *J Am Ceram Soc*. 2017;100:2199–2208.